

PREDICTION OF THE THERMAL SPALLING RISK OF CONCRETE STRUCTURES EXPOSED TO HIGH TEMPERATURES

Dariusz GAWIN ^a, Francesco PESAVENTO ^b

^a Associate Professor; Tech. University of Lodz, Lodz, Poland
E-mail address: gawindar@p.lodz.pl

^b Dr. Assistant Professor; University of Padova, Padova, Italy
E-mail address: pesa@dic.unipd.it

Received: 03.12.2008; Revised: 05.01.2009; Accepted: 02.02.2009

Abstract

A very characteristic mode of concrete damage at high temperature, especially for the materials characterized by a low intrinsic permeability, like for example HPC or UHPC, is so called thermal spalling. In this paper the results of simulations performed with a mathematical model, which considers concrete as multiphase porous material, are applied to define some spalling indexes based on various collapse mechanisms. A validation of the quantities proposed, carried out by means of a comparison with some experimental test results, is presented. Moreover, the results of a simulation dealing with a structural element exposed to a parametric fire, including a cooling phase, usually not considered in analyses, is described and discussed.

Streszczenie

Termiczne odpryskiwanie betonu (ang. thermal spalling) jest bardzo charakterystyczną formą zniszczenia tego materiału pod wpływem wysokiej temperatury. Zagrożone są zwłaszcza materiały o niskiej przepuszczalności, jak na przykład betony wysokiej i bardzo wysokiej wytrzymałości. W niniejszej pracy, bazując na modelu matematycznym betonu, traktowanego jako wielofazowy materiał porowaty, zdefiniowano pewne liczby kryterialne (tzw. indeksy spallingu), które charakteryzują niebezpieczeństwo wystąpienia termicznego odpryskiwania betonu, przy założeniu różnych mechanizmów zniszczenia materiału. Przedstawiono także wyniki eksperymentalnej weryfikacji zaproponowanych kryteriów zniszczenia betonu w wysokiej temperaturze. Ponadto opisano i przedyskutowano wyniki symulacji dotyczących betonowych elementów konstrukcyjnych, poddanych działaniu parametrycznego pożaru, z uwzględnieniem fazy studzenia konstrukcji.

Keywords: Concrete structure; High temperature; Thermal spalling; Damage; FE simulations.

1. INTRODUCTION

During heating of concrete, one observes several complex, interacting physical and chemical phenomena resulting in significant changes of the material inner structure and properties. It is commonly known that these changes can lead to a decline of load-bearing capacity or other important service features of concrete structures, especially during a rapid or/and prolonged, increase of ambient temperature, like for example during a fire or a nuclear accident. An interesting phenomenon, very specific for concrete and of a great practical importance is so called thermal

spalling which can sometimes be explosive in nature. This has been studied, both experimentally and theoretically, for many years, but its physical causes are still not fully understood and their relative significance is controversial. The reason of such a situation are inherent technical difficulties associated with testing of concrete elements at high temperature, especially when changes of physical properties and several parameters are to be measured simultaneously, e.g. the temperature and pressure fields, the moisture content, the strength properties, the intrinsic permeability etc., during experiments at controlled conditions. Usually, only fragmentary data are available from such tests

and it is very difficult to deduce from their results a full picture of the analysed phenomena. A useful tool for interpretation and better understanding of many complex phenomena, and sometimes the only possible one, can be computer simulations. However, one should remember that such an interpretation possesses all limitations and simplifications that are assumed in the mathematical model the simulation is based on. Thus, for this purpose one should use models considering possibly the whole complexity and mutual interactions of the analysed physical processes. Hence, in case of concrete at high temperature, a proper choice may be a model based on mechanics of multiphase porous media, taking into account chemical reactions (dehydration), phase changes, cracking and thermo-chemical material degradation, as well as their mutual couplings and influence on the hygral, thermal, chemical and mechanical properties of concrete. Such a kind of model was developed by the Authors in the past years and it is capable to capture the global realistic behaviour of concrete under the above described severe conditions. In the next sections a brief description of this model and its application to the definition of a relevant spalling index will be presented. Furthermore, a numerical simulation of a structural concrete member exposed to a parametric fire including the cooling phase will be described and discussed. The latter computation aims at showing the additional damage one can observe during the stage of fire suppression in which the temperature can diminish very rapidly.

2. MODELLING OF CONCRETE AS MULTIPHASE POROUS MATERIAL

The equations of the model are written by considering concrete as a multi-phase porous material, i.e. a medium whose pores are filled with more than one fluid. In the present case the solid skeleton voids are filled partly with liquid water and partly with a gas phase.

Below the critical temperature of water, T_{cr} , the liquid phase consists of physically bound water and capillary water, which appears when the degree of water saturation exceeds the upper limit of the hygroscopic region. Above the temperature T_{cr} the liquid phase consists of bound water only. In the whole temperature range the gas phase is a mixture of dry air and water vapour, which is a condensable gas constituent for temperatures $T < T_{cr}$. The constituents are assumed to be chemically non-reacting except for the solid phase which is formed by the aggregates and the

products of cement hydration (C-S-H gel and calcium hydroxide, mainly); it is hence affected by dehydration process for temperatures exceeding about 105°C. The solid phase is assumed to be in contact with all fluids in the pores.

The global multiphase system is treated in [1-3] within the framework of averaging theories, starting from microscopic level and applying the mass-, area- and volume averaging operators to the local form of balance equations, [1-3]. As underlined in [4], the interfaces between the constituents and their thermodynamic properties are of importance to consider properly constitutive relationships, thus they were taken into account in [3, 5] in the definition of the general form of the model and in the exploitation of the second law of the Thermodynamics.

Exploring this law, applied for the multi-phase porous medium, whose skeleton experiences chemical reactions (dehydration) and material deterioration (both thermo-chemical and mechanical damage) it is possible to define several important quantities used in our model (e.g. capillary pressure, net effective stress tensor of the solid phase) and obtain some thermodynamic restrictions imposed on the evolution equations for the skeleton dehydration and deterioration processes, [3-5]. The whole procedure is presented in detail in [1] and in [3-5] for a more expanded functional dependence of the internal free energy. From this approach one obtains at equilibrium state the following simplified form of the capillary pressure p^c , [4, 5]:

$$p^c = p^g - p^w \quad (1)$$

in which p^g and p^w are the gas and water pressure respectively. In the hygroscopic region (i.e. for low moisture contents when water is present only as a thin film), the thermodynamic solid pressure p^s at equilibrium can be expressed by a simplified formula neglecting the term related to the thickness of the meniscus surface (valid when the film thickness is smaller than the radius of curvature of the solid particles, [3-5]):

$$p^s = \chi_s^w (p^g - p^w) + \chi_s^g p^g + \chi_s^w s^{sw} J_{sw} + \chi_s^g s^{sg} J_{sg} \quad (2)$$

while in the non-hygroscopic region (i.e. for moderate levels of wetting phase saturation):

$$p^s = \chi_s^w p^w + \chi_s^g p^g + \chi_s^w s^{sw} J_{sw} + \chi_s^g s^{sg} J_{sg} \quad (3)$$

where $\chi_s^{\alpha s}$ are the fractions of skeleton area in contact with water and gas, $s^{\alpha s}$ are the surface tensions between solid skeleton and the fluid phases (water

and gas) and $J_{\alpha s}^s$ are the curvature of the meniscus, ($\alpha = w, g$). p_w^w is the water reservoir pressure and n^w is the disjoining pressure. The capillary pressure like terms in Eqs. (2) and (3), accounting for a jump in pressure across the curved surface of the solid, i.e. the last two terms in the RHS of these equations, are typically not included in the expressions used for the solid phase pressure in practical applications and are neglected in our model. Taking this into account, together with the definitions of capillary pressure at different water saturation levels, and obvious identity $\alpha_i^w + \alpha_i^g = 1$, allows us to write one common expression for the solid phase pressure in the following form:

$$\alpha_i^w + \alpha_i^g = 1 \tag{4}$$

Apparently Eq. (4) is similar to the commonly used expression developed for partially saturated porous media by Bishop (that is thermodynamically inconsistent), but it has been obtained here in the framework of Rational Thermodynamics [3-6]. Moreover, it is also valid for materials with very small pores and well developed internal pore surface, where water can be present as thin film, like for example in concrete, [3, 5]. From the second law of thermodynamics it is also possible to obtain the well known Fick's law, Fourier's law and Darcy's law, which describe the diffusion of miscible components (e.g. water vapour and dry air) in the gas phase, the heat transfer by conduction and the mass transport due to gradient of gas and capillary pressure, [1-3, 7].

For the model closure several thermodynamic relations, e.g. the Kelvin equation, valid because of the assumption about the local equilibrium state, perfect gases law and Dalton's law for the description of the state of gaseous phases and for the description of partial pressure, have been used, [1-3, 7]. For a description of the properties of concrete microstructure at high temperature, e.g. intrinsic permeability-damage coupling, and for the extension of the model to temperature ranges above the critical point of water, see [8, 9].

As far as the constitutive relationships describing concrete strains are concerned, considering both mechanical and thermo-chemical deterioration processes, as well as transient thermal creep phenomena, the reader is referred to [3, 5]. Following this model, the total strain of a mechanically loaded concrete at temperature T , ϵ_{tot} , can be split into the following components:

$$\epsilon_{tot}(\mathcal{T}, T) = \epsilon_{el}(\mathcal{T}, T) + \epsilon_{th}(\mathcal{T}) + \epsilon_{chem}(\mathcal{T}) + \epsilon_{tr}(\mathcal{T}, T) \tag{5}$$

where ϵ_{el} is the elastic strain due to the "net" effective stresses, acting on the load bearing part of skeleton, \mathcal{T}_e^* , and which are caused by external load and pressure of pore fluids (i.e. liquid water and moist air), ϵ_{th} is the thermal strain component, ϵ_{chem} the thermo-chemical strain (irreversible component), and ϵ_{tr} the transient thermal strain, called also LITS [10] or thermal creep. We remind, that the shrinkage strain is included into the elastic strain component as a result of action of capillary pressure (considering disjoining pressure at lower moisture contents) upon the solid surface fraction being in direct contact with liquid water, χ_s^{ws} (S_w), dependent on the moisture content, see Eq. (4).

To describe uniquely the state of concrete at high temperature, we need 4 primary state variables, i.e. gas pressure, p^g , capillary pressure, p^c , temperature, T , and displacement vector, \mathbf{u} , as well as 3 internal variables describing advancement of the dehydration and deterioration processes, i.e. degree of dehydration, Γ^{dehydr} , chemical damage parameter, V , and mechanical damage parameter, d . Using the values of the mentioned damage parameters, the total damage parameter, D , can be calculated. The model consists of 7 equations: 2 mass balances (continuity equations), enthalpy (energy) balance, linear momentum balance (mechanical equilibrium equation) and 3 evolution equations. The final form of the model equations, expressed in terms of the primary state variables are listed below. The full development of the equations is presented in [1-3, 5, 7-9].

– *Mass balance equation of the dry air* (involving the solid skeleton mass balance) takes into account both diffusive and advective air flow, as well as variations of porosity caused by dehydration process and deformations of the skeleton. It has got the following form:

$$-\alpha \frac{D^s S_a}{Dt} - \beta_s (1-\alpha) S_a \frac{DT}{Dt} + S_a \operatorname{div} \mathbf{v} + \frac{S_a n}{\rho^s} \frac{D^s \rho^s}{Dt} + \frac{1}{\rho^s} \operatorname{div} \mathcal{J}_a^s + \frac{1}{\rho^s} \operatorname{div} (\alpha S_a \rho^s \mathbf{v}^a) - \frac{(1-\alpha) S_a}{\rho^s} \frac{\partial \rho^s}{\partial T_{solid}} \frac{DT_{solid}}{Dt} = \frac{\partial \rho_{solid}}{\partial T} S_a \tag{6}$$

– *Mass balance equation of the water species* (involving the solid skeleton mass balance) considers diffusive and advective flow of water vapour, mass sources related to phase changes of vapour (evaporation-condensation, physical adsorption – desorption and dehydration), and variations of porosity caused by dehydration process and deformations of the skeleton, resulting in the following equation:

$$\begin{aligned} & (\rho' - \rho^*) \frac{\partial S_s}{\partial t} + (\rho' S_s + \rho^* S_s) \operatorname{div} \mathbf{v}' - \beta_{swg} \frac{\partial T}{\partial t} + S_s \rho' \frac{\partial \rho'}{\partial t} = \operatorname{div} \mathbf{q}' + \\ & + \operatorname{div} (\kappa S_s \rho' \mathbf{v}') + \operatorname{div} (\kappa S_s \rho^* \mathbf{v}') - (\rho' S_s + \rho^* S_s) \frac{(1-\pi)}{\rho'} \frac{\partial \rho'}{\partial t} - \frac{\partial \dot{m}_{dehydr}}{\partial t} = \\ & = \frac{\partial \dot{m}_{dehydr}}{\partial t} (\rho' S_s + \rho^* S_s - \rho') \end{aligned} \quad (7)$$

with β_{swg} defined by:

$$\beta_{swg} = \beta_s (1-\pi) (S_s \rho'^2 + S_s \rho'^2) + \pi \beta_s S_s \rho' \quad (8)$$

– *Enthalpy balance equation of the multi-phase medium*, accounting for the conductive and convective heat flow, and heat effects of phase changes and dehydration process, can be written as follows:

$$\begin{aligned} & (\rho C_p)_{eff} \frac{\partial T}{\partial t} + (\rho_s C_p^s \mathbf{v}' + \rho_s C_p^s \mathbf{v}^*) \cdot \operatorname{grad} T - \operatorname{div} (\chi_{eff} \operatorname{grad} T) = \\ & = -\dot{m}_{dehydr} \Delta H_{dehydr} + \dot{m}_{dehydr} \Delta H_{dehydr} \end{aligned} \quad (9)$$

where χ_{eff} is effective conductivity from experiments, and

$$\begin{aligned} \dot{m}_{dehydr} & = -\rho' S_s \operatorname{div} \frac{\partial \mathbf{u}}{\partial t} + \beta_{swg} \rho' \frac{\partial T}{\partial t} - \rho' \pi \frac{\partial S_s}{\partial t} + \\ & - \operatorname{div} \left[\rho' \frac{\mathbf{k} k^*}{\mu'} (-\operatorname{grad} \phi' + \operatorname{grad} \phi' + \rho' \mathbf{g}) \right] + \\ & - \left(\dot{m}_{dehydr} + (1-\pi) \frac{\partial \rho'}{\partial t} \frac{\partial \Gamma_{dehydr}}{\partial t} \right) \frac{\rho' S_s}{\rho'} + \dot{m}_{dehydr} \end{aligned} \quad (10)$$

with: $\beta_{swg} = S_s [(1-\pi)\beta_s + \pi\beta_u]$

and the dehydrated water source is proportional to the dehydration rate:

$$\dot{m}_{dehydr} = k_b \dot{\Gamma}_{dehydr} \quad (11)$$

k_b is a material parameter related to the chemically bound water and dependent on the stoichiometry of the chemical reactions associated to dehydration process.

– *Linear momentum conservation equation of the multi-phase medium* has the following form:

$$\operatorname{div} (\boldsymbol{\sigma}' - \alpha \rho' \mathbf{I}) + \rho \mathbf{g} = \mathbf{0} \quad (12)$$

where $\alpha = 1 - K_T/K_S$ is Biot’s coefficient and the effective stress is given by:

$$\boldsymbol{\sigma}' = (1-d')(1-V) \boldsymbol{\Lambda}_s : (\boldsymbol{\epsilon}_{tot} - \boldsymbol{\epsilon}_a - \boldsymbol{\epsilon}_{dehydr} - \boldsymbol{\epsilon}_s) \quad (13)$$

– *Dehydration process evolution law*, considering its irreversibility, has the form:

$$\dot{\Gamma}_{dehydr}(t) = \dot{\Gamma}_{dehydr}(T_{max}(t)) \quad (14)$$

where $T_{max}(t)$ is the highest temperature reached by

the concrete up to the time instant t .

The constitutive relationship $\dot{\Gamma}_{dehydr}(T_{max}(t))$ can be obtained from the results of thermo-gravimetric (TG or DTA) tests, using the definition of the dehydration degree by means of the mass changes during concrete heating:

$$\dot{\Gamma}_{dehydr}(T) = \frac{m(T_o) - m(T)}{m(T_o) - m(T_\infty)} \quad (15)$$

where $m(T)$ is mass of concrete specimen measured at temperature T during TG tests, T_o and T_∞ are temperatures when the dehydration process starts and finishes. We assumed here $T_o = 105^\circ\text{C}$ and $T_\infty = 1000^\circ\text{C}$.

– *Thermo-chemical damage evolution equation*, obtained on the basis of the experimental results, takes into account the irreversible character of the material structural changes and may be written as, [5, 7]:

$$\dot{V}(t) = \dot{V}(T_{max}(t)) \quad (16)$$

– *Mechanical damage evolution equation*, of the following form:

$$\dot{d}(t) = \dot{d}(\dot{\epsilon}(t)) \quad (17)$$

is expressed in terms of the equivalent strain, $\dot{\epsilon}$, given by equations of the classical non-local, isotropic damage theory, [11-13]. The parameters of the theory can be determined from the results of the strength tests (“stress - strain” curves) at various temperatures, [7, 13].

The governing equations of the model are discretised in space by means of the Finite Element method and in time domain by applying a Finite Differences scheme [1, 5, and 7].

The model described above has been successfully applied to the case of fire in tunnels [14] and to the assessment of fire damage in concrete structures exposed to high temperature and to protecting/repairing techniques [15, 16].

3. ASSESSMENT OF THE THERMAL SPALLING RISK

In this section we recall and briefly discussed some quantitative criteria which can be useful for assessment of the risk that spalling occurs. Such criteria have been already proposed in the past by several researchers [17-23], but most of them were formulat-

ed on an experimental basis only, often in the form of diagrams showing “area of the spalling risk”, as a function of various concrete properties, e.g. permeability, tensile strength, etc., hence their validity was limited to the materials and element geometries (shapes and dimensions) used in the tests they were based on. There were also some attempts to formulate some analytical criteria, e.g. using limit state analysis [19, 21], but they were usually based on simplified models of concrete performance during heating, by evaluating the thermally induced stresses and/or vapour pressures. A systematic analysis of the criteria proposed by several authors in the past is beyond the scope of this paper. Herein, only a schematic classification and brief description of these criteria is presented. They can be subdivided in three main categories:

1. Criteria based on pore pressure prediction, which consider the pore pressure as responsible for thermal spalling, [22]. Usually, the models employed for the description of the hygral state of concrete are rather simple. For example, mass transport in concrete pores is considered as a purely diffusive phenomenon, or pore pressure is directly evaluated by using an idealized spherical model for the pores of the material [20]. In some cases so-called “moisture clog” is indicated as the main cause of spalling [18].
2. Criteria based on thermal stresses. These are the simplest ones and are related to the non uniform thermal strains that can result in stresses equal to the maximum compressive strength of concrete for a given temperature, e.g. [17].
3. Criteria based on combined action of thermal stresses and pore pressure. This class of spalling criteria encompasses the criteria by Zhukov [19] and Connelly [21]. The first author has proposed a method for the evaluation of the strain energy density in the direction of the heated surface W_x , taking into account the stresses due to external mechanical load, thermal field and pore pressure acting on a slab heated on one face. The spalling occurs when the strain energy density W_x in x -direction equals the rupture energy density defined on the basis of tensile strength of concrete. Connelly [21] has extended Zhukov’s model considering pore pressure stresses as acting simultaneously in the three directions x,y,z . The critical state for spalling is defined in a way similar to Zhukov’s approach.

In both the aforementioned methods the mechanical

behaviour of concrete is described in a simplified manner. In fact, the definition of the criterion is based on the assumption that the material behaves elastically, neglecting thermo-chemical degradation of concrete and non-linear effects, e.g. due to cracking. In the approaches presented above, the criteria omit the complexity of hygro-thermal and chemo-physical processes in concrete at high temperature hence they were not able to give a realistic evaluation of the thermal spalling risk.

3.1. Hypotheses concerning mechanisms of thermal spalling

To assess the thermal spalling risk, a detailed knowledge of several local parameters describing hygro-thermal state of concrete, stresses and strains in every point of an analysed structure is necessary. However, thermal spalling is also a “macro” phenomenon, depending on several geometrical and physical parameters of the whole structure, hence an analysis on this scale seems to be necessary, as well. Thus, it is necessary to assume some simplifying hypotheses concerning mechanisms leading to thermal spalling, based on mechanical models, which allow us to formulate some quantitative criteria useful in assessment of the risk of the phenomenon to occur.

In [16] our analysis of these spalling criteria were based on the results of computer simulations performed by means of the numerical model presented in section 2, as well as the results of the experimental tests [25, 26]. In particular three criteria were defined, assuming different macro-mechanisms leading to concrete spalling, and one “heuristic” criterion deduced from the analysis of physical processes during heating of concrete (see [16]) and the results of some experiments at these conditions, [10, 25]. All these criteria are based on detailed data concerning the evolution in time of the variables describing material deterioration, strength properties, gas pressure and hygro-thermal state in every point of the analysed structure. Some geometrical parameters, necessary in the “macro-mechanical” analysis were been deduced from the results of the experiments performed at NIST [24, 25] which were numerically modelled.

The mechanisms considered in the definition of the spalling indexes are:

The “*Pressure-induced shear model*” in which the external layer of heated concrete is considered as a simple supported beam (of length L_r and thickness b) at its ends subjected to a compression deriving from

the differential thermal dilatation. This criterion predicts the “plastic” failure of the material constraints for the external layer.

The “*Buckling model considering gas pressure*”. In this case the spalling criterion is based on the hypothesis of buckling of the compressed external layer of the structural element, previously mentioned. This layer is initially delaminated from the rest of the structure, [16] and behaves as a beam subjected to a compressive load due to thermal stresses and to a lateral pressure exerted by the gas. The collapse occurs when bending stress σ_b on the tensile side of the beam is equal to compressive thermal stress σ_{th} . Another failure mode is a compressive one which occurs if the sum of the compressive bending stress and thermal stress is equal to the compressive strength of the material.

The “*Simplified fracture mechanics model*”. This hypothesis of collapse is based on fracture mechanics. The main mechanism of compressive failure is the sideways propagation of a band of parallel axial splitting cracks. Such a kind of mechanism can lead to a sudden release of the stored elastic energy and to a modification of the original stress field, [23]. In this particular case the compressive stresses derive directly from thermal fields and the released energy is related to constrained thermal dilatation. The failure mechanism is formed by the development of two different systems of cracks: compression splitting cracks and parallel cracks in the direction of compression due to the transverse tensile stresses, Fig. 1. The global behaviour of the concrete element at macro-scale is similar to an orthotropic material. The zone affected by the energy released due to the propagation of axial splitting micro-cracks, and consequently by a relaxation of stresses, is practically a strip between parallel tensile cracks, Fig. 1.

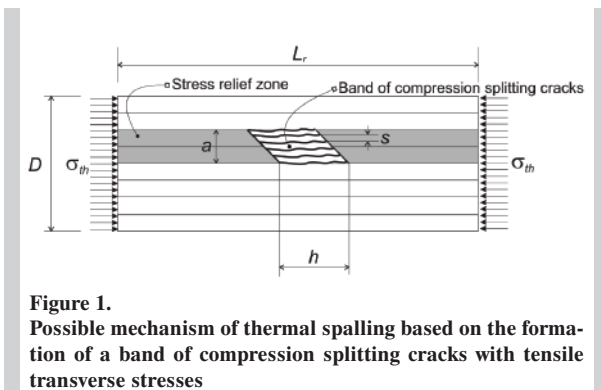


Figure 1. Possible mechanism of thermal spalling based on the formation of a band of compression splitting cracks with tensile transverse stresses

3.2. Spalling indexes

In the following a spalling index based on heuristic criteria will be introduced. Other forms of spalling indexes can be found in [16]. They are based on some collapse mechanisms briefly recalled in the previous section and that are defined and described in detail in [16]. These indexes allow for a quantitative assessment of the spalling risk. Their possible values range from 0 to 1, but presumably they cannot be interpreted as the thermal spalling probability. Five different spalling indexes have been defined, assuming different simplified models of the spalling mechanism (i.e. pressure induced shear, buckling and fracture mechanics), or considering the main key factors influencing development of the phenomenon. For the sake of completeness these indexes are listed hereafter, but only the last one will be defined and used in the calculations.

The spalling index I_{S1} , based on the pressure-induced shear model, takes into account the following parameters: the gas pressure difference between the current position and the surrounding air, the averaged (from the heated surface to a given position) traction strength, and the mechanical damage parameter. The internal geometry is described by the L_r/b ratio, where L_r is the length of compressed zone and b its thickness. The spalling index I_{S2} , based on the buckling mode of damage, considers: the local values of gas pressure and mechanical damage parameter, as well as averaged values of the Euler’s stress, the compressive stress in the surface layer, and the compressive strength. The internal geometry is defined by the $(L_r/b)^2$ ratio. The spalling index I_{S3} , based on fracture mechanics, with internal geometry characterised by the $L_r \cdot s/h$ ratio, takes into account the averaged values of elastic energy and specific energy of fracture, and local value of damage parameter. The ratio s/h characterizes micro-geometry of a fracture, [16].

The spalling indexes I_{S4} and I_{S5} are heuristic and consider the following key factors favouring development of the thermal spalling: high local values of the gas overpressure, $p^g - p_{atm}$, and mechanical damage parameter, d , and high, averaged (from the heated surface to a given position) values of transversal traction stresses, $\bar{\sigma}_{th}$, and constrained elastic energy, \bar{U} . The factors impeding thermal spalling are high, averaged values of traction strength, \bar{f}_t , and specific fracture energy, \bar{G}_f . The spalling index I_{S5} has the same form as I_{S4} , defined by:

$$I_{S5} = \frac{\bar{\sigma}_{th} \cdot \bar{U} \cdot d}{\bar{f}_t \cdot \bar{G}_f} \cdot \frac{p^g - p_{atm} \cdot L \cdot C_f}{p_{atm}} \quad (18)$$

but it omits effect of the specific fracture energy. The index I_{ss} , indicated as I_s in the following, is the only one used in the calculations described in the next sections.

4. RESULTS OF NUMERICAL SIMULATIONS

4.1. Simulation of NIST laboratory test

To analyze the thermal spalling risk, we have performed, with the numerical model presented in section 2, computer simulations, based on the NIST laboratory tests [24, 25], for four different types of concrete. The cylindrical specimens, all of them with diameter of 100 mm and height of 200 mm, were tested using different test methods and target temperatures. Herein, our attention is focused on the first type of concrete called MIX1, [24, 25], whose samples were subjected to unstressed heating tests to the final target temperature (i.e. samples were first heated and then loaded). The target temperatures considered here are of 450°C and 300°C. In the first case all the specimens experienced explosive spalling, while the second temperature was not dangerous for the tested cylinders. The main material properties of the MIX1 at ambient temperature are listed in Table 1 (for further details, see [5, 16]).

During the test, heating rate was initially equal to 5 K/min and heating was stopped when the temperature in the centre of the specimen was within 10 K of the target temperature T , and the difference between the surface and centre temperatures of the concrete specimen was less than 10 K. For further details concerning the mix compositions and tests procedures (set-up, temperature control, instrumentation of the specimens), see [24, 25].

The results for the first case (i.e. target temperature of 450°C) were used to determine the internal geometry parameters in such a way, that the values of all spalling indexes were equal to one at the time and position corresponding to their real values during the tests [24, 25]. Using the results of our simulations, we determined the evolutions of mechanical damage parameter, gas pressure and elastic energy of constrained strains, which are considered to be the key factors influencing thermal spalling risk, as well as the spalling indexes, for the analyzed concrete mix.

Exemplary results, concerning the spalling index I_s , the mechanical damage and the gas pressure are presented in Fig. 2. As can be seen, the obtained values of spalling index indicate much higher risk of the thermal spalling occurrence for the case of target temperature equal to 450°C than for the one of 300°C, what is in a good agreement with the experiment. The selected time stations

correspond to the one before the peak of the spalling index, the one at time instant of the peak and the one after spalling index reached the maximum value. For all the other spalling indexes the obtained results were similar, but the most precise indication of the time and position of the spalling was obtained for the I_{ss} index, which was not possible considering simply the mechanical damage evolution, Fig. 2B. For a complete description of the test case the reader is referred to [16].

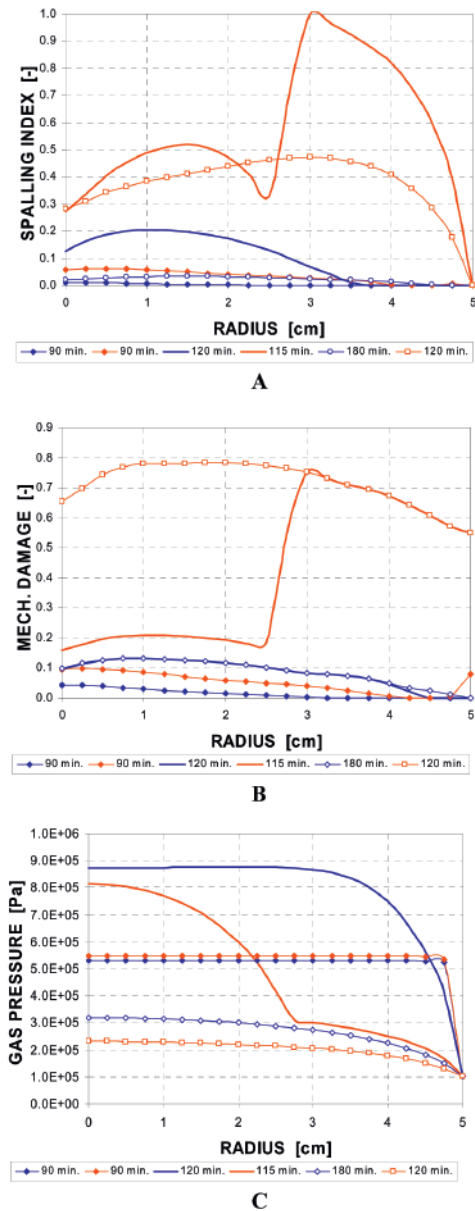


Figure 2. Comparison of the evolution of spalling index I_s (a) mechanical damage (b) and gas pressure obtained from the simulation of the NIST tests [24, 25], for the two analyzed cases: 450°C (red lines) and 300°C (blue lines)

4.2. Fire of high-rise building with fast cooling

The model presented in section 2 has been applied here to the calculation of some structural elements of high rise buildings, more precisely a concrete column exposed to a fire described by a parametric heating profile.

The latter one can be obtained from the time-temperature parametric curves defined in the Eurocode 1, Part 1-2 [26], formulated on experimental basis. The time-temperature parametric curves defined in the Annex A of the Eurocode 1, Part 1-2 [26] are, on the contrary to the nominal curves, dependent on certain physical parameters such as for example:

- The fire load density (the higher fire load density the longer the fire is),
- The ventilation conditions, depending mainly on the geometry, size and distribution of the compartment openings (big ventilation openings lead to fast fires but less severe),
- The properties of the closing walls of the fire compartment (walls gain energy and limit the fire temperature).

These curves also differ from the nominal curves in the sense that after a heating stage they show a cooling one (see below), and they are valid for fire sectors with a built surface not higher than 500 square meters, without holes at the roof and with a maximum height of 4 meters, assuming a complete combustion of the fire load.

They are defined in the heating stage by:

$$\Theta_g = 20 + 1325 \cdot (1 - 0.324 \cdot e^{-0.118t^*} - 0.284 \cdot e^{-1.4t^*} - 0.472 \cdot e^{-2.18t^*}) \quad (19)$$

where Θ_g [°C] is the air temperature within the fire sector, while t^* is a sort of equivalent time (in hours) that takes into account not only the time, but also so called “opening coefficient”. This parameter can be calculated from the area of total surface of the vertical openings, the total surface closing the fire sector, the averaged height of the windows at all of the walls and the characteristics of the material (specific heat, thermal conductivity and mass density). For further details about the definition of the possible profiles from the parametric curves, see [26]. From a general viewpoint, when the fire is controlled by the ventilation conditions the increase of the opening coefficient leads to shorter but more severe fires, until fires are controlled by the thermal load. From this point the influence of the opening coefficient is especially observed on the cooling rate of the environment. It is

recalled that a fire is defined as “ventilation controlled” if the peak of temperature (calculated on the basis of the fire load density and the opening coefficient) takes place at times longer than a limit value of time t_{lim} (equal to 15, 20 or 25 minutes for slow, medium speed and fast development, respectively). If $t_{max} \leq t_{lim}$ the fire can be classified as “fire load”.

By starting from the previous considerations, the heating profile selected for the calculation of the structural element is the following:

$$\Theta_g = 20 + 1325 \cdot (1 - 0.324 \cdot e^{-0.118t^*} - 0.284 \cdot e^{-1.4t^*} - 0.472 \cdot e^{-2.18t^*}) \quad (20)$$

that is shown in Fig. 4 (solid blue line noted as “ T_{env} ”) and that corresponds, for the chosen material, to the minimum value of the opening coefficient allowed in the European rules (i.e. 0.02 m^{1/2}).

The heating stage defined with the profile (20) is followed by a cooling phase defined under the same considerations. It is a fast cooling for which the environmental temperature decreases very quickly (within 20 seconds) from the maximum (i.e. about 709.5 K, reached in 80 minutes) down to the initial value, after a stationary stage at the maximum for 2 minutes. This condition corresponds to the case of a rapid intervention of the firemen. Hence, the cooling profile is mathematically formulated as follows:

$$\Theta_g = 406.362 - 30.3681 \cdot (t - 4020) \quad (21)$$

As far as the boundary conditions are concerned, a mixed convective-radiative condition has been assumed with a convective exchange coefficient equal to 20 W/m²K and an emissivity equal to 0.9. The mass exchange between the surface of the concrete element and the environment is characterized by a convective flux. The water vapour pressure is kept constant (equal to 1300 Pa). During heating this corresponds to a rapid decrease of the ambient relative humidity down to zero. The mass exchange coefficient is set to 0.025 m/s.

Figure 3 shows the size of the cross section of the square column under consideration (30×30 cm). The properties of the material (C60) assumed in the simulation are listed in Table 1.

Figure 4 shows the temperature histories in six different points located at various depths from the heated surfaces of the column. The sharp decrease of environmental temperature, due to the cooling, leads to a rapid decrease of the temperature in these points, especially those close to the lateral sides of

Table 1.
Main properties of the materials at 20°C

Material property	MIX1	C60
Water / binder ratio, w/b [-]	0.22	0.33
MIP porosity, n [%]	7.7	8.25
Water intrinsic permeability, k_o [m ²]	2×10^{-19}	2×10^{-18}
Young modulus, E [GPa]	37.2	34.4
Compressive strength, f_c [MPa]	79.5	60
Thermal conductivity, λ [W/m·K]	2.5	1.92
Specific heat, C_p [J/kg·K]	800	855

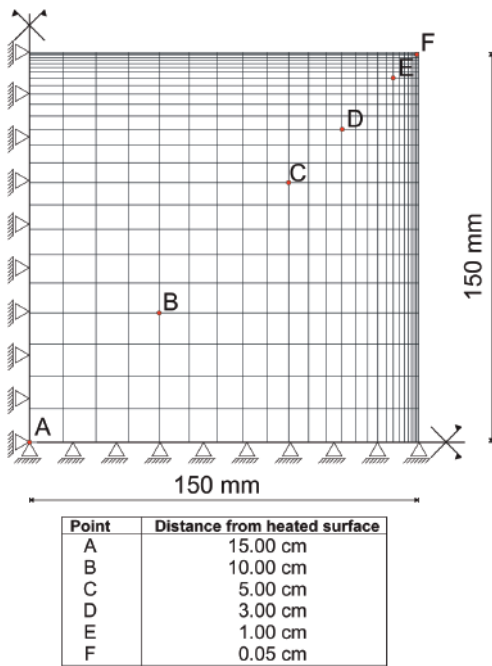


Figure 3.
Cross section of the square column: geometry and FE mesh used in the computations

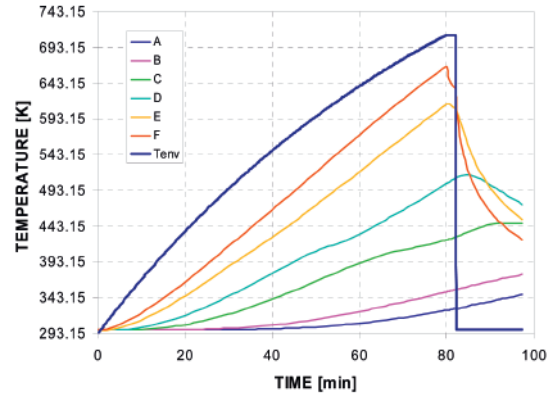


Figure 4.
Temperature histories in the environment (solid blue line), and in points A, B, C, D, E, F at various depths from the heated sides

the cross section. The inversion of thermal fluxes has important consequences not only from the thermo-hygral point of view, but also for the mechanical behaviour of the material.

In Figure 5A one can observe the distribution of temperature at $t = 80$ min, corresponding to the time instant of maximum heating. Fig. 5B represents the temperature distribution at the end of the computation (approximately 100 minutes). The decrease of temperature is of about 200 K.

Figs. 6A and 6B show the distribution of the relative humidity at the two time stations chosen. Again the maximum values of RH are attained at the end of the heating phase in the inner part of the cross section whereas the outer part is almost completely dried. After cooling the relative humidity in the core of the column has values close to the initial ones while the

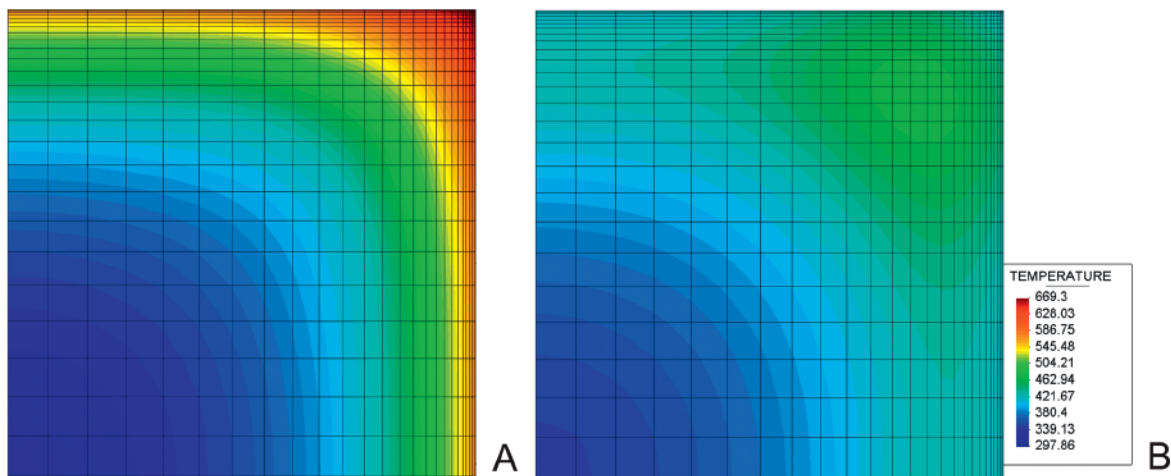


Figure 5.
Distributions of the temperature [K] at 80 min (A) and at the final time (B)

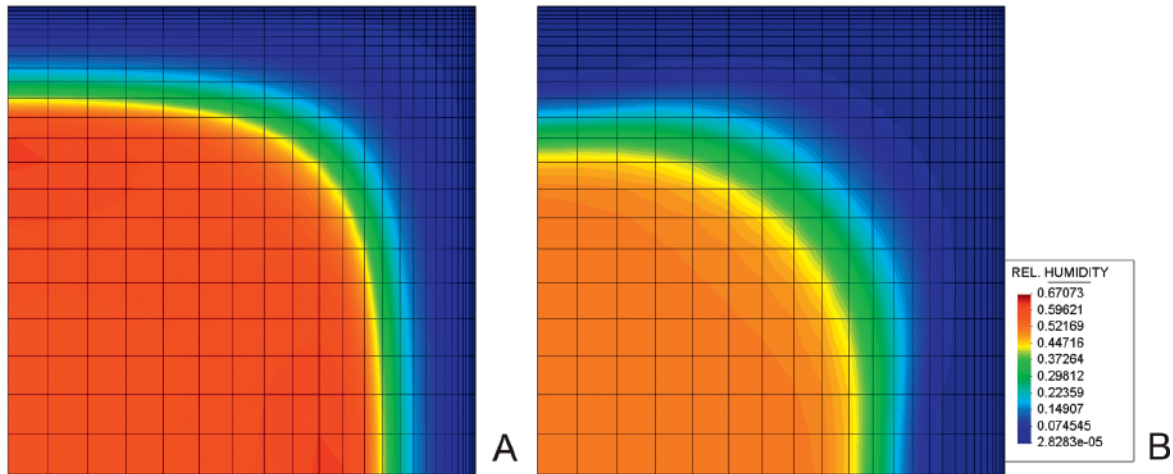


Figure 6.
Distributions of the Relative Humidity [-] at 80 min (A) and at the final time (B)

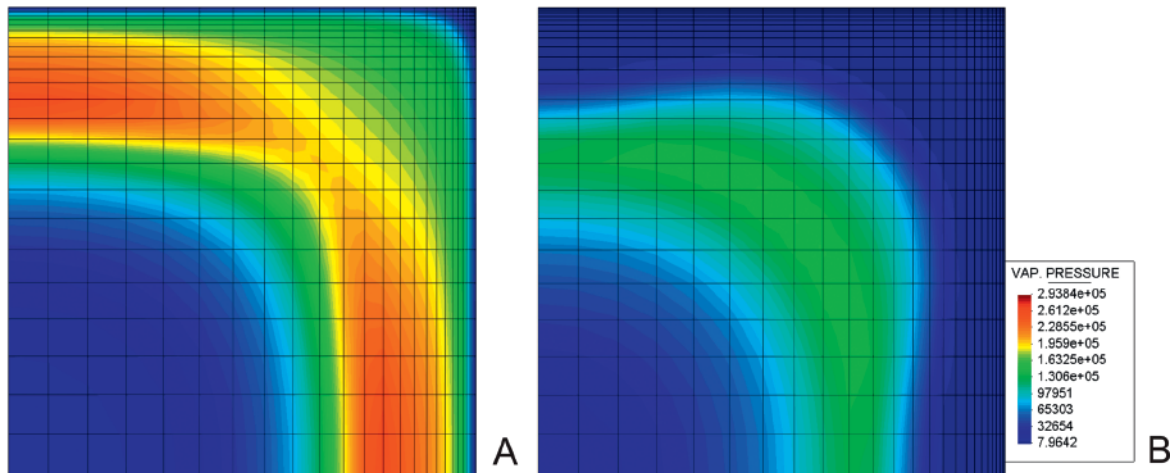


Figure 7.
Distributions of the vapour pressure [Pa] at 80 min (A) and at the final time (B)

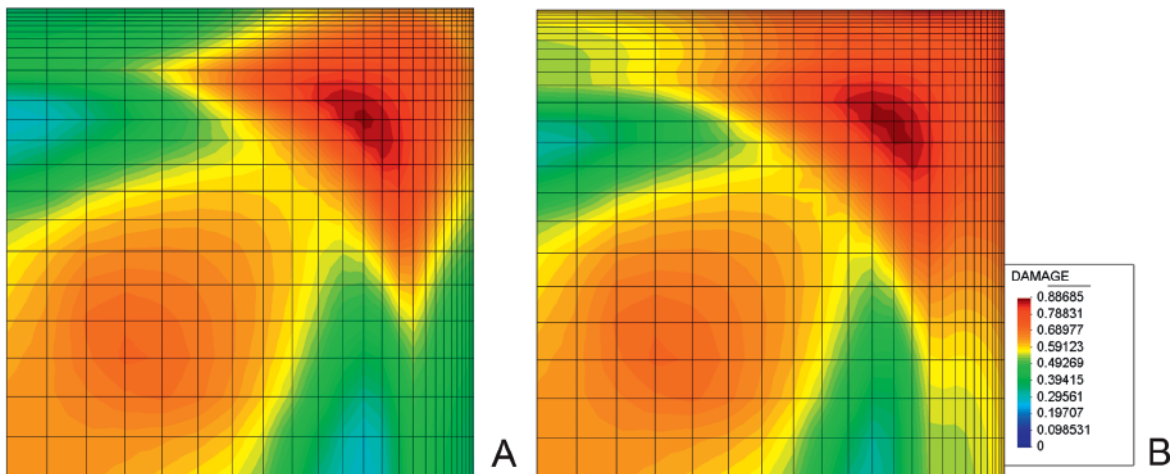


Figure 8.
Distributions of the damage [-] at 80 min (A) and at the final time (B)

external part is almost fully dried. From these maps one can figure out that drying is progressing also during the cooling phase.

Vapour pressure distribution at 80 min and at the end of calculation is depicted in Figs. 7A and 7B. In this case it is worthy to notice the influence of the damage on the pressure value: the pressure peaks are concentrated in the zones characterized by a lower value of damage parameter, Fig. 7A. The pressure is lower where the material is deeply damaged (i.e. close to the corner). At the end of the process the pressure is almost uniformly distributed throughout the cross section of the column and its values are no higher than 1 bar, Fig. 7B.

Finally, in Figs. 8A and 8B one can observe the distribution of damage parameter. Unlike temperature and other thermo-hygral quantities, the damage is continuously increasing because of an additional damaging of the material even during the cooling phase. In Fig. 8B it is clearly visible that the zone of damaged concrete is larger than the one in Fig. 8A, (i.e. before cooling).

4. CONCLUSIONS

The presented simulations showed that the proposed spalling indexes can be used for assessment of the thermal spalling risk. These indexes are based on different assumptions concerning the thermal spalling mechanisms or key factors affecting the phenomenon, but their predictions are quantitatively similar as shown in [16]. The tested spalling indexes are calculated by using the results of our computer simulations concerning the evolutions of gas pressure, temperature, mechanical and thermo-chemical damage parameters, stresses, elastic energy of elastic strains, etc. They allowed to predict the time and position of the thermal spalling occurrence, being in a good agreement with the NIST experiment. During assessment of damage caused by a fire one should take into account not only the heating phase of fire but also the cooling one because degradation phenomena can develop further even when the element surface temperature decreases as the numerical simulation showed.

REFERENCES

- [1] *Pesavento F.*; Non linear modelling of concrete as multiphase porous material in high temperature conditions, PhD thesis, University of Padova, Padova (Italy), 2000
- [2] *Schrefler B.A., Pesavento F.*; Multiphase flow in deforming porous material, *Computer and Geotechnics*, Vol.31, 2004; p.237-250
- [3] *Pesavento F., Gawin D., Schrefler B.A.*; Modelling cementitious materials as multiphase porous media: theoretical framework and applications, *Acta Mech*, DOI:10.1007/s00707-008-0065-z, Vol.201, 2008; p.313-339
- [4] *Gray W.G., Schrefler B.A.*; Thermodynamic Approach to Effective Stress in Partially Saturated Porous Media, *Eur. J. Mech. A/Solids*, Vol.20, 2001; p.521-538
- [5] *Gawin D., Pesavento F., & Schrefler B.A.*; Modelling of deformations of high strength concrete at elevated temperatures, *Mat. Struct.*, Vol.37, No.268, 2004; p.218-236
- [6] *Gray W.G., Schrefler B.A., Pesavento F.*; The solid phase stress tensor in porous media mechanics and the Hill-Mandel condition, *Int. J. Physics and Mechanics of Solids*, in press. *Acta Mechanica* paper
- [7] *Gawin D., Pesavento F., & Schrefler B.A.*; Modelling of hygro-thermal behaviour of concrete at high temperature with thermo-chemical and mechanical material degradation, *Comput. Methods Appl. Mech. Engrg.*, Vol.192, 2003; p.1731-1771
- [8] *Gawin D., Pesavento F., & Schrefler B.A.*; Simulation of damage-permeability coupling in hygro-thermo-mechanical analysis of concrete at high temperature, *Commun. Numer. Meth. Engrg*, Vol.18, No.2, 2002; p.113-119
- [9] *Gawin D., Pesavento F., & Schrefler B.A.*; Modelling of hygro-thermal behaviour and damage of concrete at temperature above the critical point of water, *Int. J. Numer. Anal. Meth. in Geomech.*, Vol.26, No.6, 2002; p.537-562
- [10] *Khoury G.A.*; Strain components of nuclear-reactor-type concretes during first heating cycle, *Nuclear Engineering and Design*, Vol.156, 1995; p.313-321
- [11] *Mazars J.*; Description of the behaviour of composite concretes under complex loadings through continuum damage mechanics, *Proc. of Tenth U.S. National Congress of Applied Mechanics*, J.P. Lamb (ed.), 1989; ASME
- [12] *Pijaudier-Cabot J.*; Non Local Damage, H.B. Mühlhaus (ed.), *Continuum models for materials with microstructure*, Wiley & Sons, Chichester, 1995; p.105-143

- [13] *Gawin D., Pesavento F. & Schrefler B.A.*; Modelling damaging processes of concrete at high temperature with thermodynamics of multiphase porous media, *J. of Theoretical and Applied Mechanics*, Vol.44, No.3, 2006; p.505-532
- [14] *Schrefler B.A., Brunello P., Gawin D., Maiorana C.E., Pesavento F.*; Concrete at high temperature with application to tunnel fire, *Comp. Mech*, Vol.29, 2002; p.43-51
- [15] *Witek A., et al.*; Finite Element analysis of various methods for protection of concrete structures against spalling during fire, *Comp. Mech.*, Vol.39, No.3, 2007; p.271-292
- [16] *Gawin D., Pesavento F., & Schrefler B.A.*; Towards prediction of the thermal spalling risk through a multiphase porous media model of concrete, *Comput. Methods Appl. Mech. Engrg.*, Vol.195, 2006; p.5707-5729
- [17] *Saito H.*; Explosive spalling of prestressed concrete in fire, Internal Report No 22, Building Research Institute, Tokyo, Japan, 1965
- [18] *Harmathy T.Z.*; Effect of moisture on the fire endurance of building elements, ASTM special technical publication 385, Philadelphia, USA, 1965
- [19] *Zhukov V.V.*; Explosive failure of concrete during a fire, (in Russian). Translation No DT 2124, Joint Fire Research Organization, Borehamwood, 1975
- [20] *Sullivan P.J., Akhtaruzzaman A.A.*; Explosive spalling of concrete exposed to high temperature, *Proc. of First International on Structural Mechanics in Reactor Technology*, Berlin, 1971
- [21] *Connolly R.J.*; The spalling of concrete in fires, PhD thesis, Aston University, 1995; p.294
- [22] *Khoylou N.*; Modelling of moisture migration and spalling behaviour in non-uniformly heated concrete, PhD thesis, Imperial College, London, 1997; p.1147
- [23] *Bazant Z.P., Planas J.*; Fracture and size effect in concrete and other quasi-brittle materials, CRC Press, New York, 1998
- [24] *Phan, L.T.*; Fire performance of high-strength concrete: a report of the state-of-the-art, Research Report NISTIR 5934, NIST, Gaithersburg, 1996
- [25] *Phan L.T., Lawson J.R., Davis F.L.*; Effects of elevated temperature exposure on heating characteristics, spalling, and residual properties of high performance concrete, *Materials and Structures*, Vol.34, 2001; p.83-91
- [26] UNE-EN 1991-1-2, Eurocode 1: G. Parte 1-2: Azioni generali. Azioni su strutture esposte al fuoco (General actions – Actions on structures exposed to fire), Maggio 2004